

M3D-skin: Multi-material 3D-printed Tactile Sensor with Hierarchical Infill Structures for Pressure Sensing

Shunnosuke Yoshimura¹, Kento Kawaharazuka^{1,2}, and Kei Okada¹

Abstract—Tactile sensors have a wide range of applications, from utilization in robotic grippers to human motion measurement. If tactile sensors could be fabricated and integrated more easily, their applicability would further expand. In this study, we propose a tactile sensor—M3D-skin—that can be easily fabricated with high versatility by leveraging the infill patterns of a multi-material fused deposition modeling (FDM) 3D printer as the sensing principle. This method employs conductive and non-conductive flexible filaments to create a hierarchical structure with a specific infill pattern. The flexible hierarchical structure deforms under pressure, leading to a change in electrical resistance, enabling the acquisition of tactile information. We measure the changes in characteristics of the proposed tactile sensor caused by modifications to the hierarchical structure. Additionally, we demonstrate the fabrication and use of a multi-tile sensor. Furthermore, as applications, we implement motion pattern measurement on the sole of a foot, integration with a robotic hand, and tactile-based robotic operations. Through these experiments, we validate the effectiveness of the proposed tactile sensor.

I. INTRODUCTION

Tactile sensors are widely utilized across various fields, ranging from control and recognition tasks in robotic object grasping [1], [2] to human motion analysis in wearable devices [3], [4]. In these applications, improving the ease of integration and enabling rapid and simple development of tactile sensors would enhance their usability and expand their range of applications.

The primary sensing principles for tactile sensors include piezoresistive, capacitive, and piezoelectric methods [5]–[8]. However, these approaches often require specialized fabrication techniques and may present challenges in terms of shape customization, scalability, and adaptability. To address these issues, research has explored tactile sensors fabricated using rubber molding and 3D printing [9]–[15]. In particular, if a widely accessible sensor could be created using fused deposition modeling (FDM) 3D printing and general-purpose materials, it would significantly contribute to the widespread adoption of tactile sensing technologies.

In this study, we propose a tactile sensor, M3D-skin, which utilizes the infill patterns of FDM 3D printers. An overview of the concept is shown in Fig. 1. This approach involves alternating layers of conductive and non-conductive flexible filaments printed with a specific infill pattern, forming a

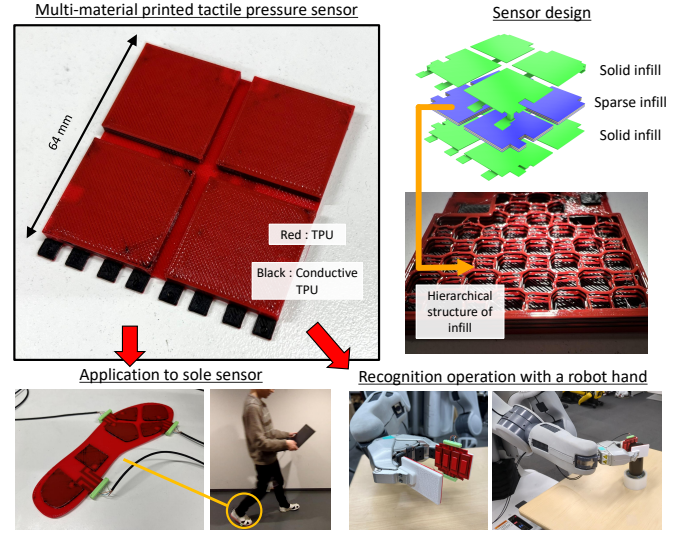


Fig. 1. Overview of this study. The upper section illustrates the 3D-printed tactile sensor, M3D-skin, including its structure and internal infill pattern. The lower section presents application examples of the sensor.

hierarchical structure. The deformation of this hierarchical structure under applied pressure induces a change in electrical resistance, allowing for the acquisition of tactile information. Additionally, an embedded wiring layer enables the creation and use of arbitrarily shaped, multi-tile sensors.

In our experiments, we first measure the sensor's characteristics and evaluate how different hierarchical structures affect its performance, demonstrating their properties and adjustability. Next, we fabricate multi-tile sensors to verify their usability. Finally, as applications of this sensor, we implement motion pattern detection on the sole of a foot and integrate it into a robotic hand for tactile-based operations. These experiments demonstrate that the proposed sensor can be easily and cost-effectively fabricated using an FDM 3D printer while enabling arbitrary shapes and multi-tile configurations, as well as excellent integration and applicability.

A. Related Work

The primary sensing principles for tactile sensors include piezoresistive, capacitive, and piezoelectric methods. Various hybrid and novel sensor designs have been proposed, such as a capacitive–piezoresistive hybrid pressure sensor [5] and an electrically resistive pressure sensor utilizing a porous and microstructured piezoresistive material [6]. Additionally, a high-sensitivity MEMS capacitive pressure sensor that separates pressure sensing and capacitance measurement [7]

¹ The authors are with the Department of Mechano-Informatics, Graduate School of Information Science and Technology, The University of Tokyo, 7-3-1 Hongo, Bunkyo-ku, Tokyo, 113-8656, Japan. [yoshimura, kawaharazuka, okada]@jsk.t.u-tokyo.ac.jp

² The author is with the AI Center, Graduate School of Information Science and Technology, The University of Tokyo, Japan.

and a piezoelectric sensor leveraging a kirigami structure [8] have been developed. Furthermore, new sensing principles using novel materials have been explored, such as ultrathin gold nanowires [16] and optical fiber pressure sensors based on polarization-maintaining photonic crystal fiber [17].

To develop more easily integrable tactile sensors, research has explored fabrication using rubber molding and 3D printing. A PolyJet-based 3D-printed integrated robotic hand and sensor system [9] enables pressure distribution measurement through image recognition. Other approaches include pressure sensors combining Hall sensors with printed structures [10], stretchable force sensors printed with silicon-based materials [11], flexible pressure sensors based on piezoresistive composites fabricated with custom FDM printers [12], and highly sensitive pressure sensors utilizing printed structures combined with elastomers [13].

For simpler, lower-cost, and shape-customizable fabrication, an integrated sensor using commercial FDM 3D printers and readily available filaments is ideal. Previous research includes capacitive sensors formed by layering conductive filaments [14], but they exhibit small capacitance changes. Another method uses deformable protrusions for pressure sensing [15], but the required large protrusions limit shape and size flexibility.

A key challenge in FDM 3D-printed sensor fabrication is that widely available, low-cost conductive and flexible filaments are stiffer than rubber, leading to minimal deformation under pressure. This results in small capacitance changes [14] and the need for large protrusions [15]. In contrast, this study proposes utilizing infill patterns, a unique feature of FDM 3D printing, as the pressure-sensitive structure. This approach enables significant resistance changes even with small deformations, overcoming these limitations.

II. METHOD

A. Sensor Structure

The overall structure of M3D-skin is shown in Fig. 2. It is fabricated using a FDM 3D printer with conductive and non-conductive TPU (Thermoplastic Polyurethane) filaments. This sensor consists of three structural components: a sensor layer for pressure sensing, wiring layers for consolidating the wiring, and cover layers for surface protection.

1) *Sensor Layer*: The structure of the sensor layer is shown in Fig. 3. At the core of this layer, a sensing structure is created by alternately stacking conductive and non-conductive filaments with a specific number of layers and infill pattern (Fig. 3[A]). In the 3D design data, the conductive filament layers are completely separated. Unlike standard 3D printing settings, this layer does not include solid infill on the top or bottom surfaces. Therefore, at the transition points between conductive and non-conductive filaments, the sparse infill patterns come into direct contact. Additionally, solid infill conductive filament layers are placed above and below this hierarchical structure to encapsulate it (Fig. 3[B]). The resistance measurement during compression is performed in the section between these upper and lower solid infill layers.

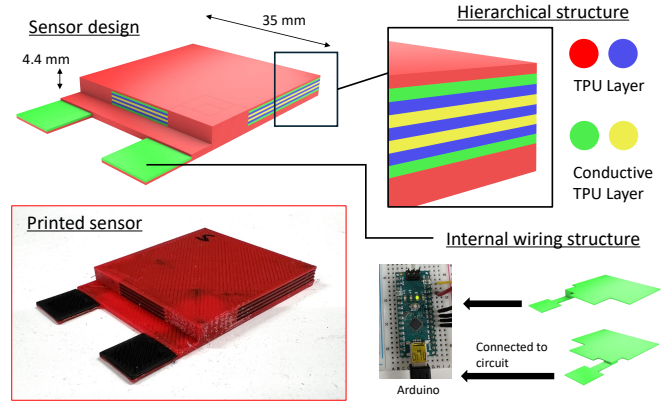


Fig. 2. The structure of M3D-skin. The upper part of the sensor performs sensing through a layered structure composed of conductive and non-conductive filaments. The lower part of the sensor includes wiring layers, which connect to the circuit.

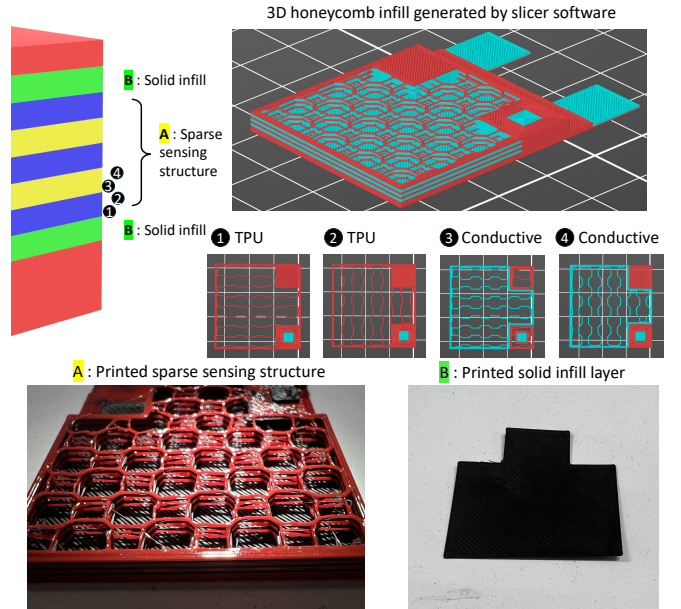


Fig. 3. The structure of the sensor layer: (A) The sparse infill sensing layer, and (B) The solid infill layers above and below the sensing layer. The sparse pattern structure utilizing infill in (A) is illustrated in the top-right of the figure, showing both the overall shape and the shape of each layer. The lower section presents the printed results of (A) and (B).

2) *Wiring Layer*: The wiring layer is shown in Fig. 4. This structure connects the upper and lower solid infill layers of the sensor layer to the underlying wiring, enabling connection to the circuit. This allows terminal connections to the circuit can be placed at any desired location, regardless of the overall shape of the sensor.

3) *Cover Layer*: The cover layer is placed above and below the sensor and wiring layers to provide surface protection. This layer is printed using standard TPU filament.

The key design parameters are listed in Table I.

B. Sensor Principle

An overview of the sensor principle is shown in Fig. 5. In the sensor layer, conductive and non-conductive filaments

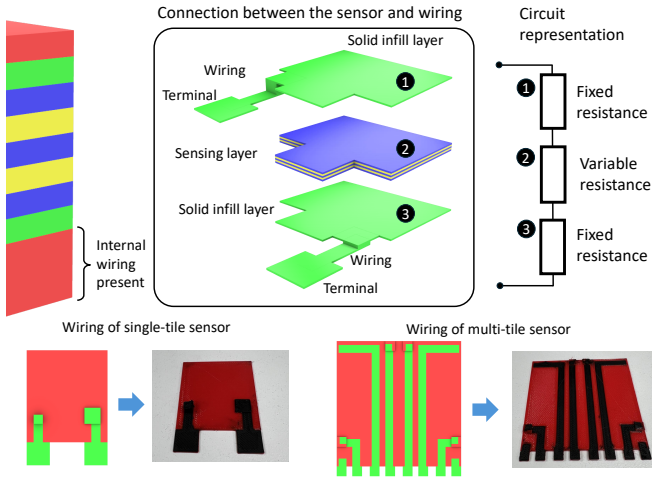


Fig. 4. The structure of the wiring layer. It connects the upper and lower infill layers of the sensor layer to the terminals. The resistance between the terminals is the sum of the resistance of the infill layers, wiring, and sensor layer. The lower section of the figure shows wiring examples for a single-tile sensor and a four-tile sensor.

TABLE I
BASELINE DESIGN PARAMETERS

Parameter	Value
Sensor Layer Conductive Filament Thickness	0.4 mm
Sensor Layer Non-Conductive Filament Thickness	0.4 mm
Sensor Layer Number of Patterned Layers	4
Wiring Layer Thickness	0.4 mm
Cover Layer Thickness	0.4 mm
Layer Height	0.2 mm
Nozzle Diameter	0.4 mm
Sensor Layer Infill Density	10 %
Sensor Layer Infill Pattern	3D Honeycomb
Sensor Layer Wall Thickness	0.8 mm
Infill Density (Outside Sensor Area)	100 %

are alternately stacked. In the 3D design data, the conductive filament layers are completely separated because they are interleaved with non-conductive filament layers above and below. However, when this structure is printed with a sparse infill pattern, overhangs and printing instabilities cause portions of the conductive filament to protrude into the adjacent non-conductive filament layers. As a result, even in the undeformed state, the conductive filament layers establish electrical continuity with the adjacent layers. When pressure is applied to this structure, the sparse and flexible infill pattern deforms. This deformation increases the contact area between conductive filament layers, leading to a change in electrical resistance.

It should also be noted that the total resistance measured between the sensor terminals includes both the resistance of the sensor layer and the resistance of the wiring layer. Thus, the measured terminal resistance is the sum of the wiring layer resistance and the sensor layer resistance. A shorter wiring layer reduces its contribution to the total resistance, making the sensor's resistance change more pronounced and improving its usability.

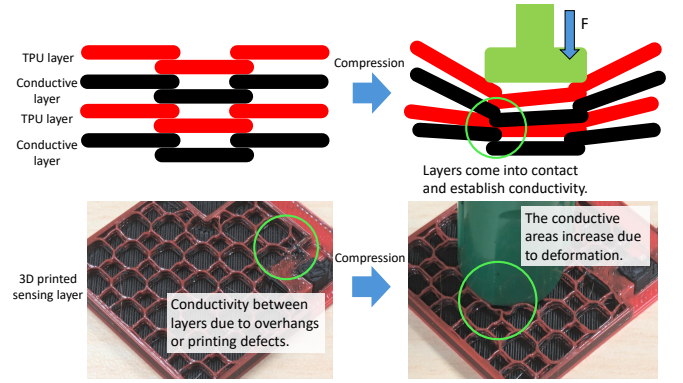


Fig. 5. Illustration of the sensor principle, showing how the infill structure deforms under compression.

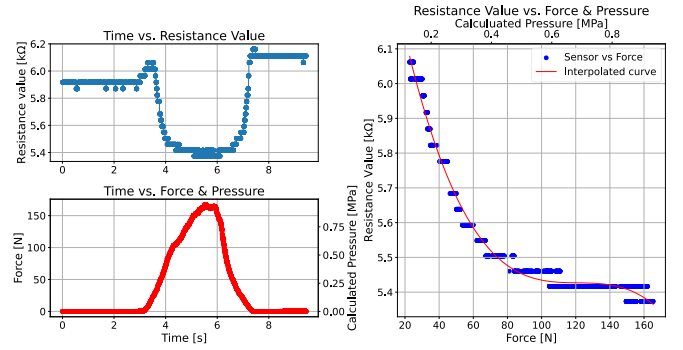


Fig. 6. Change in resistance when the sensor is subjected to an external force.

C. Design and Fabrication

The three-dimensional structure of this sensor is uniquely determined by specifying parameters such as the planar area of its shape and the thickness of the stacked layers. In this study, to enable rapid design for arbitrary shapes and different parameters, we have systematized the design process using parametric modeling with Rhinoceros and Grasshopper. This allows for the fast design of sensor layer structures tailored to specific applications.

For 3D printing, we used the Prusa XL 5-toolhead [18], a multi-material, tool-changer-based 3D printer. The non-conductive filament used for printing was TPU 95A, while the conductive filament (Conductive Filaflex) was TPU 92A. The sensor is fabricated in a single integrated printing process, eliminating the need for preprocessing, post-processing, or assembly.

III. EXPERIMENT

A. Sensor Characterization

First, we fabricated M3D-skin based on the shape shown in Fig. 2 and the parameters listed in Table I, and measured its characteristics. A force was applied to the center of the sensor using a force gauge with a 15 mm-diameter circular tip, and the changes in resistance were measured via a voltage divider circuit connected to an Arduino. The results are presented in Fig. 6.

On the left side of the figure, the time variations of force and resistance are shown. In the undeformed state, the

resistance is about 5.9 k Ω . As force is applied, the resistance increases to around 6.1 k Ω up to approximately 25 N, then decreases to about 5.4 k Ω up to 160 N. When the applied force is reduced, the resistance returns, reaching 6.1 k Ω once the force is back to 0 N. Even when no external force is applied, the resistance remains roughly 0.2 k Ω higher than the initial state, but gradually decreases over time until it returns to its original value. This residual resistance change is believed to occur because internal deformation remains after a large force is removed and only gradually reverts to its original state.

Next, the right side of Fig. 6 shows the relationship between force (and pressure) and resistance in the interval from $t = 3.5$ s to $t = 5.5$ s, during which the force is applied. Although the resistance change is significant up to about 100 N and 0.6 MPa, it becomes smaller thereafter, gradually changing up to around 160 N. Compared to the initial resistance of around 6 k Ω , the change is about 0.6 k Ω , which is sufficiently large for the Arduino and voltage divider circuit to measure and detect.

B. Relationship Between Structure and Characteristics

The characteristics of the sensor with different structural configurations are shown in Fig. 7 and Fig. 8.

1) *Structural and Parameter Modifications:* First, the left side of Fig. 7 shows the characteristics when the layered structure is removed, and the entire sensor layer is made of conductive filament. In this case, the resistance change is extremely small, demonstrating that the layered structure of conductive and non-conductive filaments is essential for the sensor to function properly. Next, the center of Fig. 7 presents the case where the number of layered structures is increased. The baseline parameter consists of four conductive layers, but when the number of layers is reduced to three, the resistance change becomes smaller. Conversely, in the case of five layers, the initial resistance is higher, and the resistance change is particularly large in the 60–100 N range, but the sensor becomes less responsive to smaller forces. This indicates that increasing the number of layers results in a greater resistance change upon compression, while also modifying the range of detectable forces. Finally, the right side of Fig. 7 shows the characteristics when the sensor layer is printed without walls. Compared to the baseline parameters with walls, the resistance change is larger, and the sensor is more sensitive to small forces below 20 N. The absence of walls increases the flexibility of the sensor layer, enhancing sensitivity. However, due to the reduced rigidity, the printing stability decreases, and black conductive filament contamination is observed on the sensor surface. While removing the walls improves sensitivity, it also introduces printing instability, which may lead to structural and characteristic inconsistencies.

2) *Effect of Infill Parameter Changes:* The changes in characteristics when modifying the infill pattern and density are shown in Fig. 8. The sensitivity to force and the magnitude of resistance changes differ depending on the infill pattern. For 10% infill density, the 3D honeycomb pattern

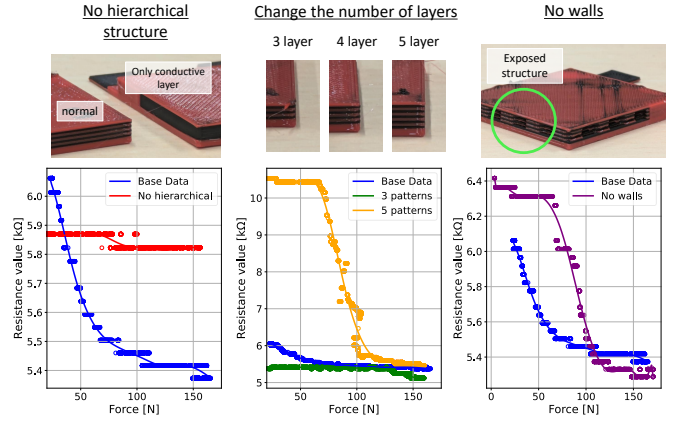


Fig. 7. Comparison of sensor characteristics with different structures and parameters. The figure presents cases where the layered structure is removed, the number of layers is modified, and the walls are removed. The blue line represents the baseline parameter for comparison.

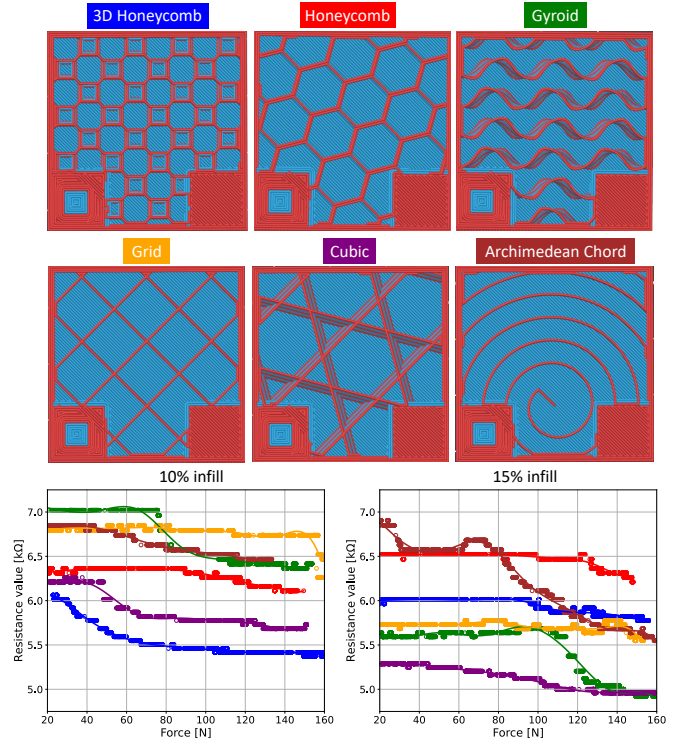


Fig. 8. Comparison of characteristics when varying infill patterns and densities. The colors of the infill names at the top correspond to the plot colors. Additionally, characteristics for 10% and 15% infill densities are shown.

demonstrates high sensitivity and stable resistance changes up to 100 N, making it well-suited as a sensor. With 15% infill density, the sensitivity range of the 3D honeycomb extends from 100 N to 160 N. The honeycomb pattern exhibits small resistance changes for both densities, likely due to its high structural strength and minimal deformation. The gyroid pattern shows significant resistance changes, but the range where resistance varies significantly is limited to approximately 40 N. The cubic pattern, particularly at 15% infill, achieves a wide sensing range. The grid and Archimedean chord patterns show resistance variations, but

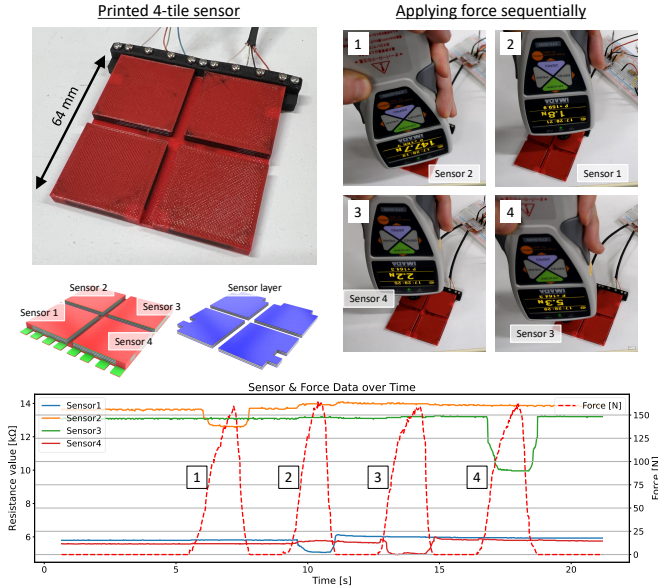


Fig. 9. Resistance change of the 4-tile sensor under applied force.

they tend to be unstable, especially at 15% infill.

These results indicate that selecting an appropriate infill pattern is crucial for achieving stable sensor characteristics. Patterns such as 3D honeycomb, gyroid, and cubic, which change shape across printing layers, exhibit greater deformation under compression due to their flexibility, making it easier to obtain resistance changes. On the other hand, if a sensor that responds only to high pressure is required, high-strength infill patterns such as the honeycomb should be chosen.

C. 4-Tile Sensor

To demonstrate the feasibility of using multiple tiles in a sensor, a 4-tile sensor was fabricated, and its resistance change was measured under applied force. The results are shown in Fig. 9, and the wiring layer is illustrated in Fig. 4. In this experiment, the four tiles were sequentially pressed using the tip of a force gauge, and the time variations of resistance and applied force were recorded. The resistance values of sensors 2 and 3 differ by approximately a factor of two from those of sensors 1 and 4, which is likely due to differences in the resistance of the wiring. Each sensor exhibited a resistance change of approximately 1 to 2 k Ω in response to applied force. These results demonstrate that multiple sensors can be integrally printed and utilized effectively using this approach.

D. Sensor Applications

As applications of the sensor, we explored its use as a foot pressure sensor and its integration into a robot hand.

1) *Foot Pressure Sensor*: The application of the sensor as a foot pressure sensor is shown in Fig. 10. In this experiment, a six-tile sensor was designed to match the shape of the sole, attached to the foot, and tested during walking and stair climbing. The pattern variations in sensor readings were measured. Since the resistance values varied

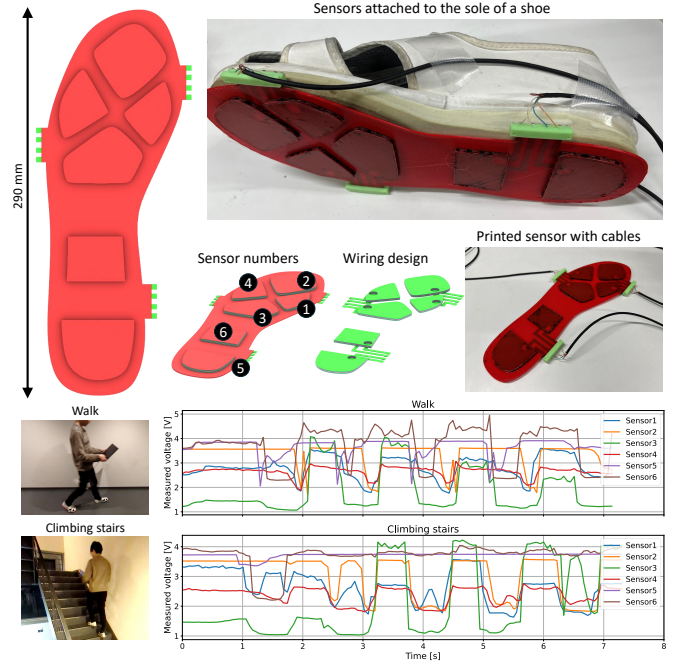


Fig. 10. Application of the sensor as a foot pressure sensor. The upper part of the figure shows the designed and printed sensor, as well as its attachment to the shoe sole. The lower part illustrates the changes in sensor readings during walking and stair climbing.

significantly across different tiles, the voltage values of the voltage divider circuit, directly read by an Arduino, were plotted for comparison. During walking, all sensors exhibited periodic changes in accordance with the walking rhythm. In contrast, during stair climbing, sensors 5 and 6, located at the heel, showed almost no change, while the other four sensors exhibited regular variations. These results indicate that the sensor can capture sufficient pattern variations corresponding to human movements. The proposed sensor is demonstrated to be useful for human motion measurement.

2) *Robot Hand*: The use of tactile sensing in a robot hand is shown in Fig. 11. In this experiment, a four-tile sensor was attached to the right hand of the dual-arm robot PR2 to perform object grasping and recognition tasks. The sensor was fabricated using single-step multi-material integrated printing, with PLA filament as the connection part to the hand, and protrusions were added to the sensor surface to enhance sensitivity. The middle section of Fig. 11 illustrates the grasping of four different objects, held either closer to the fingertips or deeper in the hand, while the corresponding sensor resistance varied from approximately 1 to 2 k Ω . The differences in resistance values among the tiles are considered to be due to variations in the resistance of the wiring sections. Next, the lower section of Fig. 11 presents an experiment in which the sensor readings during object grasping were used to determine whether the object was positioned near the fingertips or deeper in the hand, and the robot adjusted its position accordingly to insert the object into a tube. Initially, the resistance value of Sensor 2 changed, indicating that the object was located near the fingertips, leading to the determination of its position. In the second

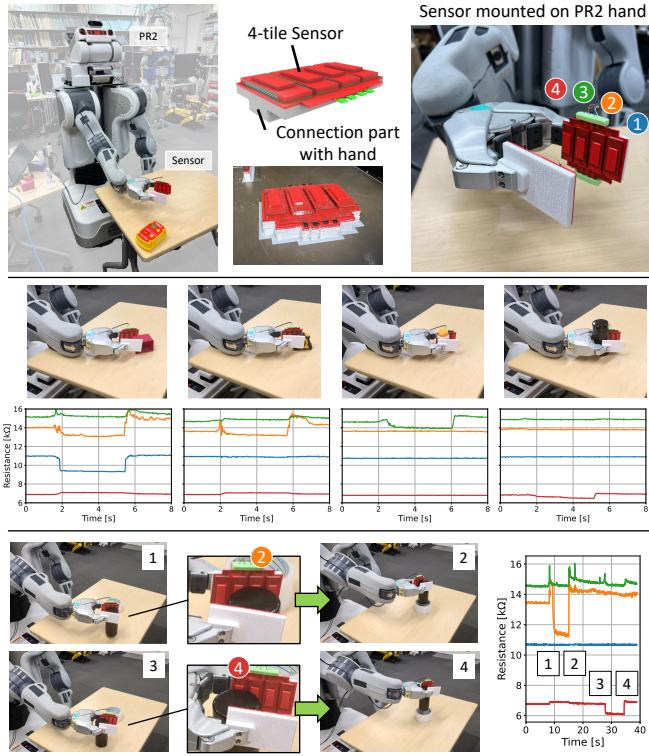


Fig. 11. Illustration of integration and recognition tasks using a robot hand. The top section shows the sensor fabricated through single-step multi-material integrated printing with conductive/non-conductive TPU and PLA, as well as its attachment to the right hand of PR2. The middle section displays the grasping of four different objects and the corresponding changes in sensor values. The lower section shows the recognition of object positions using the sensor and the subsequent action of inserting the object into a tube.

trial, the resistance value of Sensor 4 changed, indicating that the object was positioned deeper in the hand, and the position was adjusted accordingly. This experiment demonstrated not only the applicability of the sensor for robotic applications but also the feasibility of easily integrating sensors through single-step multi-material integrated printing using a 3D printer.

IV. CONCLUSION

In this study, we proposed a tactile sensor utilizing the infill patterns of layer-based 3D printing. By leveraging the hierarchical structure formed through sparse infill using conductive and non-conductive flexible filaments, we demonstrated that changes in pressure result in corresponding variations in resistance. Through experiments, we showed that the sensor's characteristics can be adjusted by modifying its structure and parameters, that multi-tile sensors can be applied to human body measurements and robotic recognition, and that easy sensor integration is possible through single-step multi-material integrated printing. These results indicate that the proposed method offers a simple, shape-adaptable, and embedded-suitable approach to tactile sensing.

Although the proposed sensor demonstrated promising performance, challenges remain in terms of durability, hysteresis handling, and improving the sensitivity range. Future prospects include developing a design methodology that con-

siders flexibility and sensitivity range as design requirements, integrating sensors with robotic components through single-step multi-material printing with a larger number of sensor tiles, and achieving more accurate pressure measurement through further analysis of sensor data.

REFERENCES

- [1] A. Schmitz, P. Maiolino, M. Maggiali, L. Natale, G. Cannata, and G. Metta, "Methods and technologies for the implementation of large-scale robot tactile sensors," *IEEE Transactions on Robotics*, vol. 27, no. 3, pp. 389–400, 2011.
- [2] W. Yuan, S. Dong, and E. H. Adelson, "Gelsight: High-resolution robot tactile sensors for estimating geometry and force," *Sensors*, vol. 17, no. 12, p. 2762, 2017.
- [3] J. C. Yeo, J. Yu, Z. M. Koh, Z. Wang, and C. T. Lim, "Wearable tactile sensor based on flexible microfluidics," *Lab on a Chip*, vol. 16, no. 17, pp. 3244–3250, 2016.
- [4] E. B. Titianova, P. S. Mateev, and I. M. Tarkka, "Footprint analysis of gait using a pressure sensor system," *Journal of Electromyography and Kinesiology*, vol. 14, no. 2, pp. 275–281, 2004.
- [5] Z. Shen, C. Yang, C. Yao, Z. Liu, X. Huang, Z. Liu, J. Mo, H. Xu, G. He, J. Tao, X. Xie, T. Hang, H.-J. Chen, and F. Liu, "Capacitive-piezoresistive hybrid flexible pressure sensor based on conductive micropillar arrays with high sensitivity over a wide dynamic range," *Mater. Horiz.*, vol. 10, pp. 499–511, 2023. [Online]. Available: <http://dx.doi.org/10.1039/D2MH00892K>
- [6] W. Li, X. Jin, X. Han, Y. Li, W. Wang, T. Lin, and Z. Zhu, "Synergy of porous structure and microstructure in piezoresistive material for high-performance and flexible pressure sensors," *ACS applied materials & interfaces*, vol. 13, no. 16, pp. 19 211–19 220, 2021.
- [7] Y. Zhang, R. Howver, B. Gogoi, and N. Yazdi, "A high-sensitive ultrathin mems capacitive pressure sensor," in *2011 16th International Solid-State Sensors, Actuators and Microsystems Conference*, 2011, pp. 112–115.
- [8] Y. Zhang, C. Liu, B. Jia, D. Ma, X. Tian, Y. Cui, and Y. Deng, "Kirigami-inspired, three-dimensional piezoelectric pressure sensors assembled by compressive buckling," *npj Flexible Electronics*, vol. 8, no. 1, p. 23, 2024.
- [9] J. W. James, A. Church, L. Cramphorn, and N. F. Lepora, "Tactile model o: Fabrication and testing of a 3d-printed, three-fingered tactile robot hand," *Soft Robotics*, vol. 8, no. 5, pp. 594–610, 2021.
- [10] J. Yu, P. B. Perera, R. V. Perera, M. M. Valashani, and A. Withana, "Fabricating customizable 3-d printed pressure sensors by tuning infill characteristics," *IEEE Sensors Journal*, vol. 24, no. 6, pp. 7604–7613, 2024.
- [11] S.-Z. Guo, K. Qiu, F. Meng, S. H. Park, and M. C. McAlpine, "3d printed stretchable tactile sensors," *Advanced materials*, vol. 29, no. 27, p. 1701218, 2017.
- [12] Z. Tang, S. Jia, C. Zhou, and B. Li, "3d printing of highly sensitive and large-measurement-range flexible pressure sensors with a positive piezoresistive effect," *ACS applied materials & interfaces*, vol. 12, no. 25, pp. 28 669–28 680, 2020.
- [13] K. Kim, J. Choi, Y. Jeong, I. Cho, M. Kim, S. Kim, Y. Oh, and I. Park, "Highly sensitive and wearable liquid metal-based pressure sensor for health monitoring applications: integration of a 3d-printed microbump array with the microchannel," *Advanced healthcare materials*, vol. 8, no. 22, p. 1900978, 2019.
- [14] M. Schouten, R. Sanders, and G. Krijnen, "3d printed flexible capacitive force sensor with a simple micro-controller based readout," in *2017 IEEE SENSORS*, 2017, pp. 1–3.
- [15] C. Massaroni, L. Vitali, D. Lo Presti, S. Silvestri, and E. Schena, "Fully additively 3d manufactured conductive deformable sensors for pressure sensing," *Advanced Intelligent Systems*, vol. 6, no. 8, p. 2300901, 2024.
- [16] S. Gong, W. Schwalb, Y. Wang, Y. Chen, Y. Tang, J. Si, B. Shirinzadeh, and W. Cheng, "A wearable and highly sensitive pressure sensor with ultrathin gold nanowires," *Nature communications*, vol. 5, no. 1, p. 3132, 2014.
- [17] H. Fu, H. Y. Tam, L.-Y. Shao, X. Dong, P. K. A. Wai, C. Lu, and S. K. Khijwania, "Pressure sensor realized with polarization-maintaining photonic crystal fiber-based sagnac interferometer," *Applied optics*, vol. 47, no. 15, pp. 2835–2839, 2008.
- [18] Prusa Research, "Original prusa xl semi-assembled single-toolhead 3d printer." [Online]. Available: <https://www.prusa3d.com/product/original-prusa-xl-semi-assembled-single-toolhead-3d-printer/>